Accepted Manuscript

Design, synthesis and SAR analysis of potent BACE1 inhibitors: Possible lead drug candidates for Alzheimer's disease

Hamadeh Tarazi, Raed Abu Odeh, Raed Al-Qawasmeh, Imad Abu Yousef, Wolfgang Voelter, Taleb H. Al-Tel

PII: S0223-5234(16)30959-X

DOI: 10.1016/j.ejmech.2016.11.021

Reference: EJMECH 9054

To appear in: *European Journal of Medicinal Chemistry*

Received Date: 6 June 2016

Revised Date: 12 October 2016

Accepted Date: 10 November 2016

Please cite this article as: H. Tarazi, R.A. Odeh, R. Al-Qawasmeh, I.A. Yousef, W. Voelter, T.H. Al-Tel, Design, synthesis and SAR analysis of potent BACE1 inhibitors: Possible lead drug candidates for Alzheimer's disease, *European Journal of Medicinal Chemistry* (2016), doi: 10.1016/j.ejmech.2016.11.021.

Graphical Abstract

Design, Synthesis and SAR Analysis of Potent BACE1 Inhibitors: Possible Lead Drug Candidates for Alzheimer's Disease

Hamadeh Tarazi,[a,b] Raed Abu Odeh,[b,c] Raed Al-Qawasmeh,[d] Imad Abu Yousef,[e] Wolfgang Voelter[f] and Taleb H. Al-Tel,[*a,b]

[a]*College of Pharmacy, University of Sharjah, P.O. Box 27272, Sharjah, UAE*

[b]*Sharjah Institute for Medical Research, University of Sharjah, P.O.Box 27272, Sharjah, UAE*

[c]*College of Health Sciences, Department of Medical Laboratory Sciences, University of Sharjah, P.O. Box 27272, Sharjah, United Arab Emirates*

[d]*Department of Chemistry, The University of Jordan, Amman 11942, Jordan*

[e]*College of Arts and Sciences, Department of Biology, Chemistry and Environmental Sciences, American University of Sharjah, Sharjah, United Arab Emirates*

[f]*Interfakultäres Institut für Biochemie, Eberhard-Karls-Universität Tübingen, Hoppe-Seyler-Straße 4, D-72076 Tübingen*

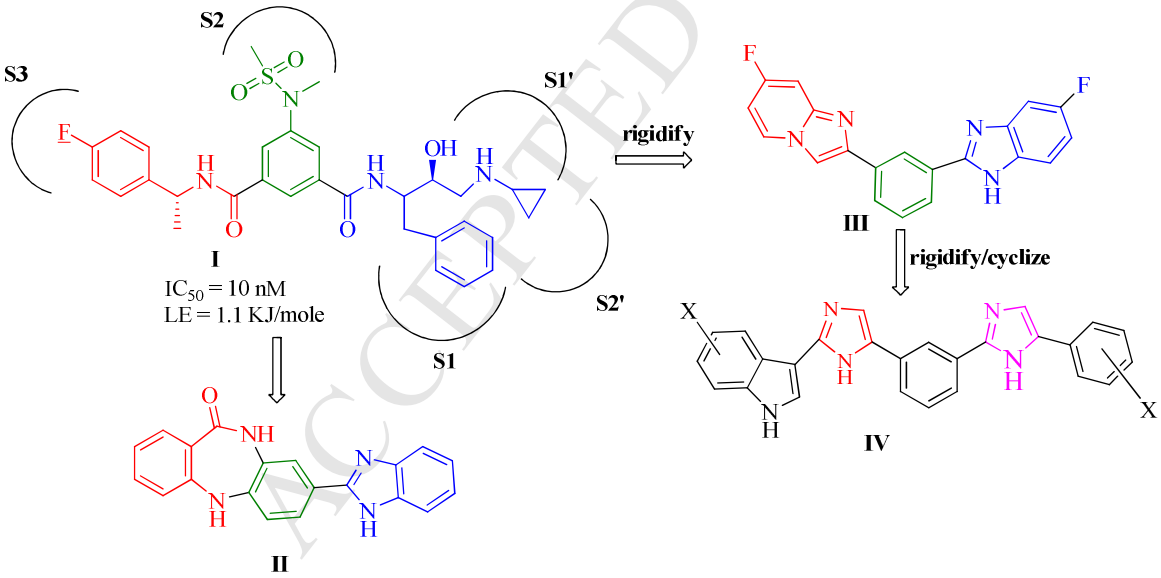

New potent isophthalic acid derivatives armed with imidazolyl and indolyl groups as β-secretase inhibitors have been synthesized. The most potent compound, **11b**, displayed an EC_{50} value of 0.29 µM.

Design, Synthesis and SAR Analysis of Potent BACE1 Inhibitors: Possible Lead Drug Candidates for Alzheimer's Disease

Hamadeh Tarazi,[a,b] Raed Abu Odeh,[b,c] Raed Al-Qawasmeh,[d] Imad Abu Yousef,[e] Wolfgang Voelter[f] and Taleb H. Al-Tel,[*a,b]

[a]*College of Pharmacy, University of Sharjah, P.O. Box 27272, Sharjah, UAE*

[b]*Sharjah Institute for Medical Research, University of Sharjah, P.O.Box 27272, Sharjah, UAE*

[c]*College of Health Sciences, Department of Medical Laboratory Sciences, University of Sharjah, P.O. Box 27272, Sharjah, United Arab Emirates*

[d]*Department of Chemistry, The University of Jordan, Amman 11942, Jordan*

[e]*College of Arts and Sciences, Department of Biology, Chemistry and Environmental Sciences, American University of Sharjah, Sharjah, United Arab Emirates*

[f]*Interfakultäres Institut für Biochemie, Eberhard-Karls-Universität Tübingen, Hoppe-Seyler-Straße 4, D-72076 Tübingen*

ABSTRACT: We have identified potent isophthalic acid derivatives armed with imidazol and indolyl groups as potent β-secretase inhibitors. The most effective analogs demonstrated low nano-molar potency for the BACE1 (β-secretase cleaving enzyme) as measured by FRET (Fluorescence Resonance Energy Transfer) and cell-based (ELISA) assays. Our design strategy followed a traditional SAR approach and was supported by molecular modeling studies based on previously reported hydroxyethylene transition state inhibitor derived from isophthalic acid **I**. In the FRET assay, the most potent compound, **10a**, displayed an IC_{50} value for BACE1 of 75 nM, and exhibited cellular activity with an EC50 value of 0.81 µM. On the other hand, compound **11b** was found to be the most potent compound in the cell-based assay with an EC_{50} value of 0.29 µM.

Keywords: β-secretase inhibitors, Alzheimer's Disease, Transition state mimics, Structure-based drug design, Structure activity relationship, Isophthalic acid derivatives.

* Corresponding author. Tel.: +971-501732950;
E-mail address: taltal@sharjah.ac.ae (T. H. Al-Tel).

1. INTRODUCTION

Alzheimer's disease (AD) is a progressive, neurodegenerative disorder and considered the most common form of irreversible dementia. To date, there are no cures that stop or reverse the underlying progression of the disease. With an aging population and increasing number of people with Alzheimer's, the need to develop ways to halt and treat the disease has become paramount [1]. According to many resources, more than 25 million people are suffering from dementia and the worldwide annual socioeconomic burden has been estimated to exceed US$200 billion [2]. As increased age is the leading risk factor of the disease, AD frequency is expected to increase to an estimated 7.7 million cases in 2030 and 11–16 million cases in 2050 in the United States alone. These numbers do not encompass the large number of people with mild cognitive impairment, a considerable proportion of whom will progress to AD [3]. Although, the cause of AD remains unknown, a large bodies of evidence that highlights the central role of Aβ in the pathogenesis of the disease [4-7]. Genetic and pathological evidences strongly support the amyloid cascade hypothesis for AD: It states that Aβ (amyloid β), a proteolytic derivative of the large transmembrane amyloid precursor protein (APP), particularly the least soluble 42 amino-acid fragment Aβ42 isoform, has an early and imperative role in all forms of AD [3] (Figure 1). Aβ–peptides are produced as a result of the sequential cleavage of APP (amyloid precursor protein), first at the N-terminus by β-secretase enzyme (β-site APP cleaving enzyme, BACE1) [8-10], followed at the C-terminus by one or more γ-secretase complexes (intramembrane aspartyl proteases) [9], as part of the β-amyloidogenic pathway. During this process, two β-secretase cleavage products are produced; a secreted ectodomain fragment named APPsol, and the membrane-bound C-terminal fragment C99 of APP [10]. Following β -secretase cleavage, a second protease, γ-secretase, cleaves C99 to generate the toxic Aβ peptides (Aβ, 39–43 residues) which are secreted from the cell. Thus, processes that limit Aβ production and deposition by preventing formation, inhibiting aggregation, and/or enhancing clearance may offer effective treatments for AD. Since β-secretase mediated cleavage of APP is the rate-limiting step of the amyloidogenic pathway, BACE1 inhibition is considered a prominent therapeutic target for treating AD by diminishing Aβ peptide formation in AD patients (Figure 1) [11-14].

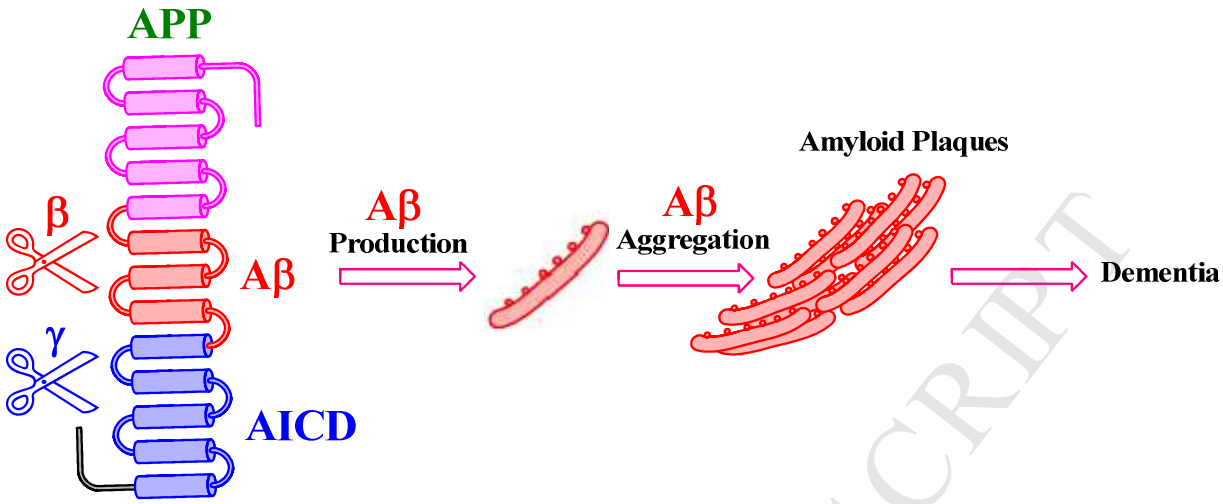

Figure 1. The amyloid hypothesis of Alzheimer's disease and proteolytic processing of the amyloid-b precursor protein (APP) leading to dementia.

The normal biological role of β-secretase is still unclear. As expected, BACE1-knockout mice are deficient in Aβ production, indicating no compensatory mechanisms for β-secretase cleavage in mice. More surprisingly, knockout mice did not exhibit serious problems due to β-secretase deletion, they were healthy, fertile, and clinical chemistry parameters were normal in both young and aged animals [15].

The absence of Aβ production and the distinct pathology in BACE1-knockout mice is encouraging for β-secretase drug development. However, inhibitor development has proven to be highly challenging, and so far, only one company has reported clinical data on a β-secretase inhibitor [16]. Most potent aspartic protease inhibitors are large hydrophilic peptides and the need for blood–brain barrier penetration adds an additional hurdle on the path towards development of a β-secretase inhibitor [17-18].

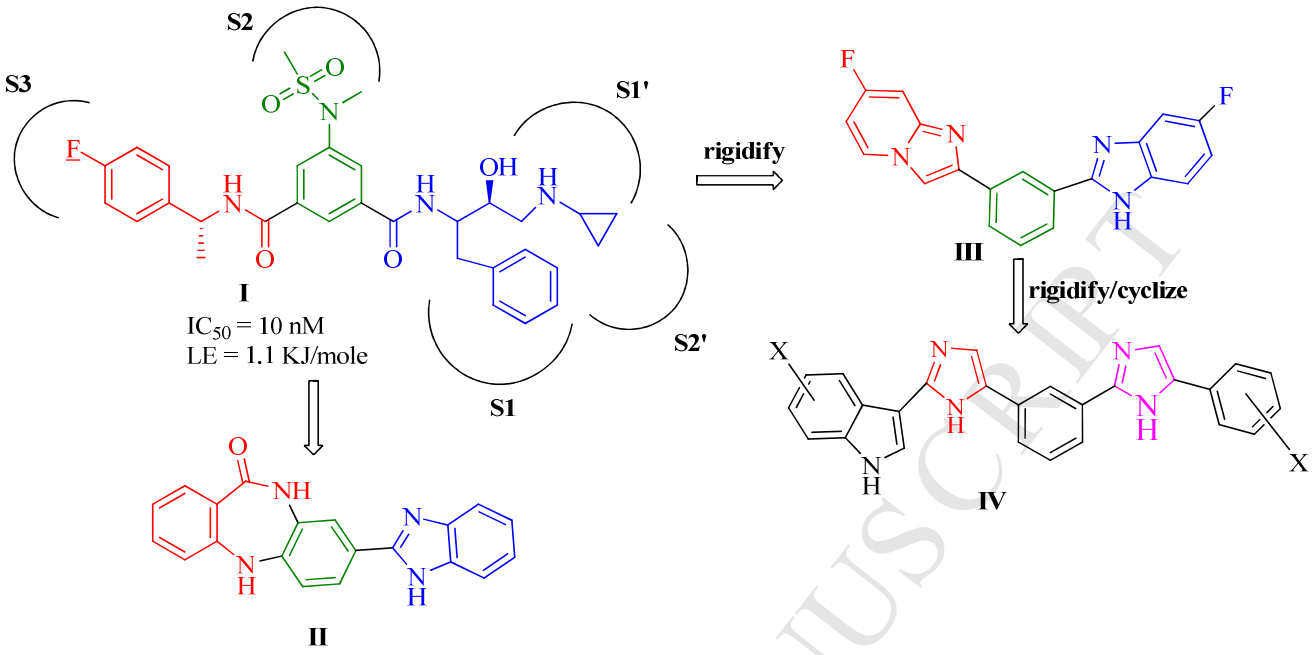

Figure 2. *De novo* design strategies utilized to find optimal fragments based on isophthalic acid motif **I**.

Recently, we have reported on the discovery of small molecules, isophthalic acid and imidazopyridine derivatives as potent BACE1 inhibitors [19-20]. From our early SAR investigations we quickly learned that the truncation of the benzamide portion on isophthalic acid **I** (Figure 2), leads to a compact scaffold **II** and proved to be a conceptually valid strategy. Soon afterwards we carried out a detailed structure-activity relationship studies around compound **I** that ultimately led to compounds of type **III** which resulted in improvement of ligand affinity for the BACE1 enzyme (IC_{50} = 20 nM; Figure 2). Furthermore, in these reports we proposed a pharmacophoric model based on isophthalic acid scaffolds that ultimately guided us in this work to efficiently design small collections of potent BACE1 inhibitors (Tables 1 and 2).

2. RESULTS AND DISCUSSION

2.1. *Chemistry*

2.1.1. *Inhibitors Design Concept*

In our previous reports we found that an imidazopyridine ring is an optimal bioisoster of the left amide appendage of compound **I**, however, an H-bond donor attached to this moiety may lead to strong interactions with the catalytic amino acid residues in the enzyme active site. At this point in time, we decided to replace the left amide portion of compound **I** by an indolyl group anchored on an imidazole

ring leading to compounds of type **IV**, hypothesizing this might improve the affinity of such motifs against BACE1. Accordingly, the IC_{50} of such motifs (**5**-**9** and **10**-**11**) ranged from 0.29 µM to 1.33 µM in the FRET assay (Tables 1 and 2). As a result, we report herein the design and synthesis of new motifs derived from isophthalic acid as potential BACE1 inhibitors. As can be concluded from Figure 2, we followed traditional medicinal chemistry strategies, among others, extension/contraction, rigidification, and bioisostere replacement to arrive at our projected motifs.

As we previously described, to improve pharmacodynamic properties for this challenging drug target, we decided to eliminate the amide functionalities of the peptide backbone present in **I** (Figure 2). To reduce the rather high flexibility of acyclic hydroxyethylene (HE) TS mimetics, the HE TS mimetic was embedded into a rigid TS mimetic (imidazole moiety cHE), retaining the essential H-bonding interactions with the aspartyl protease catalytic dyad and the Flap amino acid residues. In addition, the cyclic scaffold should provide suitable vectors for direct extensions into the corresponding S2′ and S1-S3 subpockets (Figure 4 and 5). We envisioned that this concept should provide inhibitors with enhanced potency and improved BBB permeability, due to their plausible PSA/LogP balance.

2.1.2. *Identification of Initial Candidates by Molecular Modeling*

In an iterative process, a concise set of heterocyclic scaffolds with an embedded HEA moiety and attached fragments were docked using induced-fit like protocol with FITTED modeling package. Conformational energy, S1, S2, S3 and S2′ site occupancy, and the overall binding potential were assessed, including key H bonding interactions to the catalytic residues Asp32 and Asp228, to the Flap residues. Lead differentiation and subpocket fragments were modified and scored in BACE1 active site until inhibitor candidates within the desired property limits and binding profiles were optimized.

The significant binding features exhibited by **I**, **II** and **III** in BACE-1 active site, and the poor blood brain-barrier penetrating characteristics of compound **I** prompted us to design new peptido-mimetic analogs as potent BACE-1 inhibitors applying structure-based drug design strategies: 1) Isophthalic acid from compound **I** was taken as core skeleton responsible for placing the ligands in most favorable binding mode; 2) Aryl amides, benzimidazole and aryl-anchored imidazole moieties were introduced on the isophthalic based core to form exquisite bonding with the corresponding S1-S3 pockets; 3) An indolyl group was incorporated on the left arm of the isophthalic acid scaffold to fit into the S1′ or S2′ binding pockets of BACE-1.

To confirm our hypothesis and predict accurate binding modes of designed compounds within the active pockets of BACE-1, molecular docking studies were performed as the first step. Docking BACE-1 could be a challenging task, since the enzyme reported to undergo considerable conformational changes upon ligand binding. Two regions of BACE-1 structure showed notable rearrangement upon ligand binding: The Flap region (residues 68−74) and the 10s-loop (residues 9−14) [21]. The Flap region and the 10s loop may adapt many conformations upon ligand binding: The Flap region may adapt closed or open conformations, whereas, the 10s region may adapt up or down conformations. Accordingly, selection of appropriate docking protocols would greatly affect predictions; hence we decided to tackle this by employing an induced-fit like protocol as implemented within the FITTED package.

Four BACE-1 crystal structures were selected from the protein data bank as representative structures of the enzyme conformations (Figure 3). These crystal structures were later used as basis for our fully flexible approach.

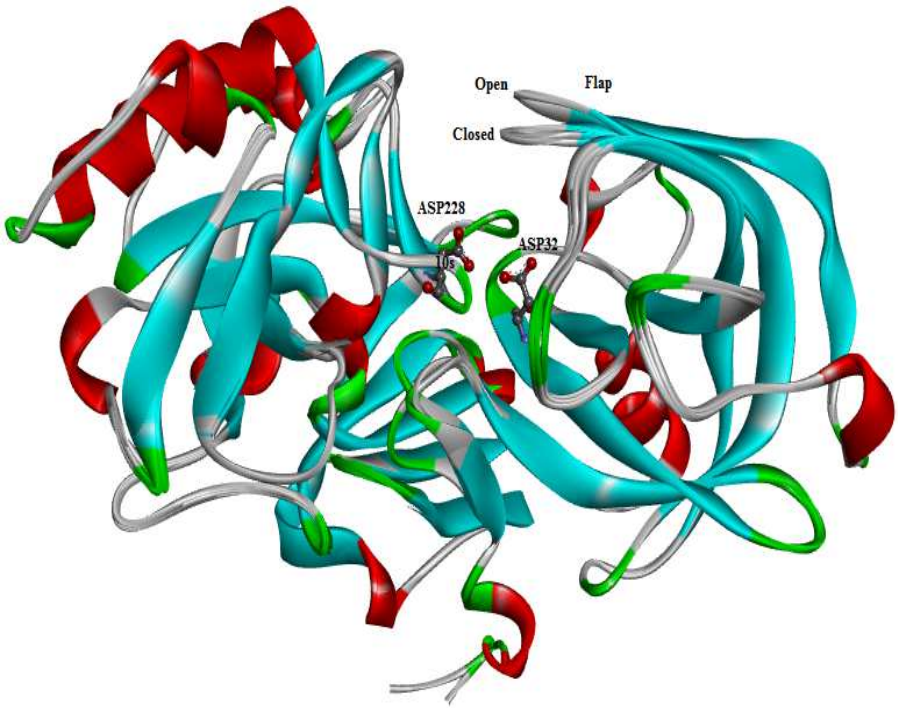

Figure 3. Overlay of four BACE-1 crystal structures (PDB-codes; 1TQF, 2B8L, 2QZL and 3EXO) illustrating the Flap, 10s region and the catalytic aspartate Dyad.

An analysis of docking results revealed that the indole arm was projected towards the amphiphilic S2′ pocket and it was engaged in direct hydrogen bonding with the catalytic residue, Asp32. This finding was observed in all of our derivatives. Based on that, we decided to use the indole group as part of the fixed scaffold and only vary the S1-S3 appendages. Therefore, four series of 3-indolyl isophathalic acid derivatives were synthesized (Schemes 1-4) and evaluated for their BACE-1 inhibitory activities.

2.1.3. *Synthesis*

We commenced our synthetic plan as contemplated in Scheme 1, we first assembled disubstituted isophthalic acid scaffolds using indole 3-carboxylic acid, **3** and compound **2**. Thus, the α-bromoketone **2** was reacted with the indolyl carboxylic acid followed by condensation with ammonia including multiple rearrangements to generate the core scaffold **I** (Figure 4). With the latter in hand, it was taken into three directional synthetic en routes to produce three series of scaffolds, **IV**, **V** and **VI** (Figure 4), thus allowing diverse prime and nonprime side structure-activity relationship (SAR) explorations needed to fit into the enzyme active site.

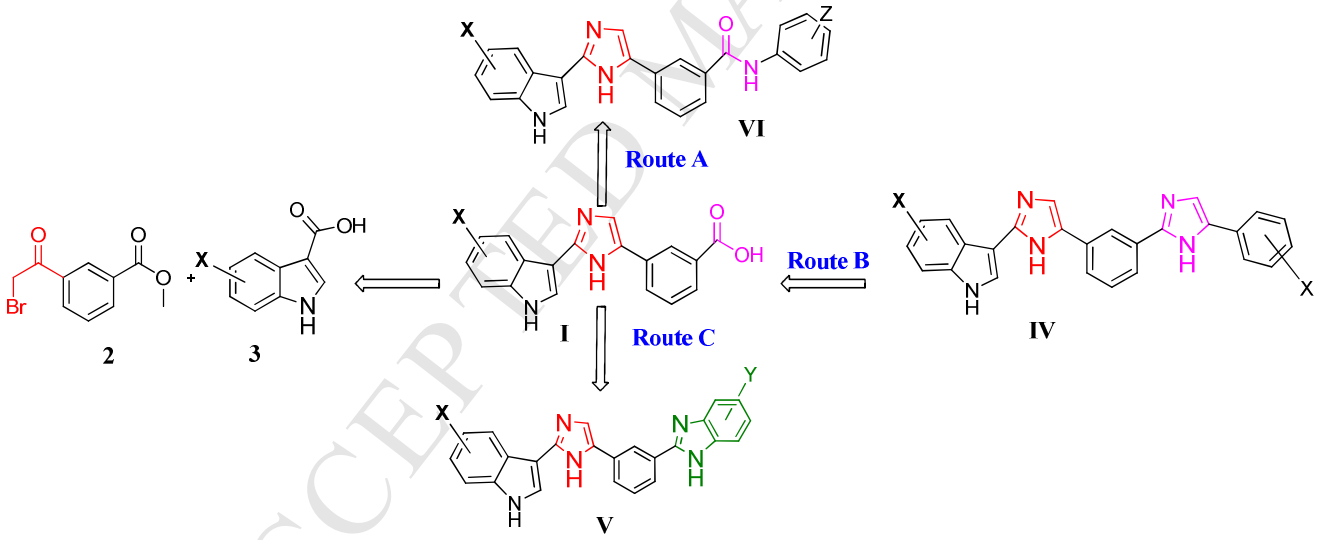

Figure 4. Retrosynthetic modifications of indolyl imidazolyl isophthalic acids scaffold

The preparation of compounds needed to delineate the SAR for this study was carried out according to synthetic Schemes 1-4. Four types of scaffolds were synthesized: In the first, indolyl-imidazoles **4a-b**, were synthesized using well established procedures [22]. The latter were coupled with the desired aniline derivative to deliver compounds **5a-d** (Scheme 1). Thus, treatment of **4a-b** with TBTU and DIPEA in DMF at 0 °C followed by addition of desired aniline, furnished compounds **5a-b** in fairly good yields.

In the second approach, compound **3** (Scheme 2) was coupled with the nitro α-bromo ketone **7** using DIPEA in DMF at 0 °C. Subsequently, the product from this step was subjected to cyclization reaction with the amidic carbonyl group via reaction with NH_4OAc in acetic acid followed by silica gel chromatography to deliver compounds **8a-b**. Subsequently, traditional reduction of the nitro group using Pd/C followed by coupling with the desired benzoic acid derivative furnished compounds **9a-b**.

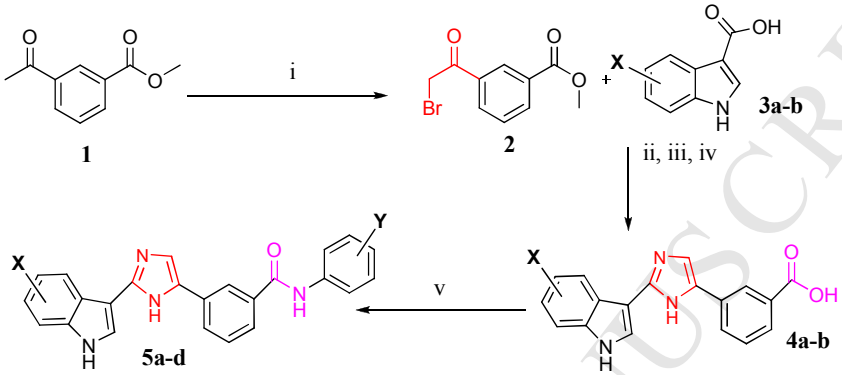

Scheme 1. Reaction conditions and reagents: (i) Br_2, DCM-MeOH; (ii) DIPEA-DMF; (iii) HCO_2NH_4, AcOH; (iv) NaOH-MeOH then H^+; (v) DIPEA, TBTU, DMF, amine.

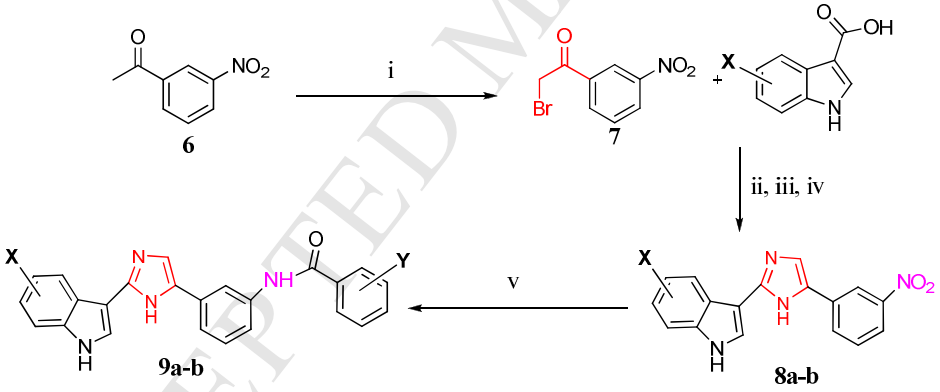

Scheme 2. Reaction conditions and reagents: (i) Br_2, DCM-MeOH; (ii) DIPEA-DMF; (iii)-HCO_2NH_4, AcOH, reflux; (iv) NaOH-MeOH then H^+; (v) Pd/C, HCO_2NH_4, MeOH, reflux.

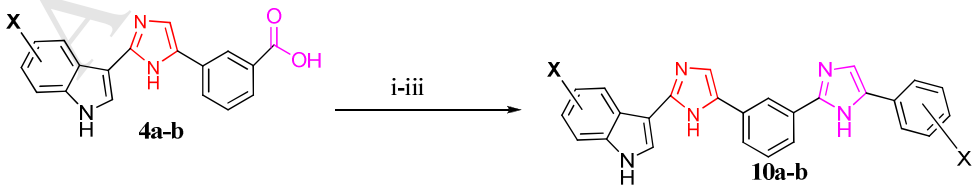

Scheme 3. Reaction conditions and reagents: (i) α-bromo ketone, DIPEA-DMF; (ii) HCO_2NH_4, AcOH, reflux; (iii) NaOH-MeOH then H^+;

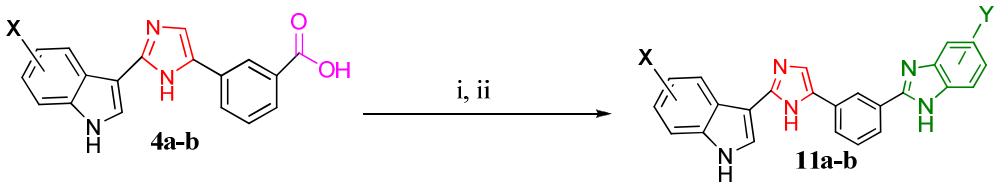

Scheme 4. Reaction conditions and reagents: (i) Phenylene diamine, TBTU, DIPEA, DMF; (ii) ACOH, reflux.

For the synthesis of the third class of compounds, namely aryl-imidazole analogs of type **10** (Scheme 3), compounds **4a-b** were reacted with the desired α-bromo ketone. Subsequently, without further purification, the products from this step were subjected to cyclization reaction with the amidic carbonyl group using NH_4OAc in refluxing AcOH followed by silica gel chromatography, to deliver compounds **10a-b**.

Having demonstrated the successful synthesis of the previous three unique collections, we next turned our attention towards the conversion of **4a-b** to more compact scaffolds. In this regard, the fourth series of compounds (Scheme 4) were synthesized using the union of phenylene diamines with the carboxylic acid derivatives **4a-b**. The products from this step were subjected to cyclization reaction through reflux in AcOH to furnish benzimidazole motifs **11a-b**.

2.2. *Biological activities and SAR analysis*

Having established robust en routes to the aforementioned compound collections, we initially profiled those for their activities against BACE1. The goal of the current study is to develop selective and potent BACE1 inhibitors. Toward this objective, we have first replaced the P1-P1' portions in compound **I** by an indolyl arm anchored on imidazole to project directly toward the S1'/S2' sub-pockets of the BACE1 active site. This was initiated based on our earlier extensive SAR analysis of compounds **II** and **III** (Figure 2). To prove that the HE transition state mimic in compound **I** could be replaced by imidazole group, we have subjected compound **I** to traditional medicinal chemistry strategies leading to scaffolds such as **IV, V** and **VI** (Figure 4). With the necessary tools needed to fully investigate the SAR in hand, the synthesized compounds were profiled for their potency at the target enzyme BACE1. The BACE1 primary screening assay utilized for this program was the fluorescence resonance energy transfer (FRET) protocol. We used

an APP-based peptide substrate (rhodamine-EVNLDAEFK-quencher, K_M value of 20 µM) carrying the Swedish mutation and containing rhodamine as a fluorescence donor and a quencher acceptor at each end. IC_{50} values were calculated by plotting the obtained relative fluorescence unit per hour (RFU/h) against the logarithmic of inhibitor concentration. The measured inhibition data were analyzed in GraphPad Prism 4 for Windows (GraphPad Software Inc., La Jolla, USA) by nonlinear regression (curve fitting). Cellular potency of advancing compounds was done *via* cell-based Aβ inhibition (Aβ40 or Aβ42) in an enzyme-linked immune sandwich assay (ELISA) in H4 cells (human neuroglioma cell line), expressing the double Swedish mutation (K595N/M596L) of human APP (APPsw). The concentration at which the cellular production of Aβ40 or Aβ42 was reduced by 50% (EC_{50}) was determined and reported in Tables 1 and 2.

Compared to compounds **I** and **II** (Figure 2), the initial simple amides as baseline analogs (e.g. **5a-d**, Table 1) showed about 20-fold less potency, when compared to compound **I** (Figure 2) and a 5-fold decrease in potency when compared to compounds of type **II** and **III**. As we were not satisfied with these results, we decided to reverse the amide appendage, as we thought this might be engaged in additional network of interactions in S1-S3 sub-pockets leading to higher affinity.

Thus, compounds **9a-b** were synthesized according to Scheme 2 and found to possess approximately similar potencies as those of **5a-d**. Interestingly, compounds **9a-b**, were found to be more potent than **5a-b** in the cell-based assay and possessed EC_{50} values of 480 and 410 nM, respectively. To understand the biological sensitivity to which compounds of types **5** and **9** were subject and to find a plausible explanation for the difference in the activity profiles between these and compound **I**, one needed to consider their docking profile in the enzyme active site. Thus, we analyzed several X-ray crystal structures of BACE1 (Figure 3) available in the Protein Data Bank and used them as a basis to calculate molecular modeling data for our compounds using the FITTED program [23] (for details see experimental section).

Based on docking modes, compounds **5a**-**5d** were found to share similar binding modes with respect to BACE-1. The aryl amide group located in the S3 pocket and the indole arm fit within the critical S2' pocket. Furthermore, we observed that the amidic and imidazole nitrogens formed additional hydrogen bonding with the corresponding near 10s loop residue, Gly230 (Figure 5a). However, for compounds with reversed amide appendage **9a-b**, two consequences were observed; firstly, the aryl amide projected toward

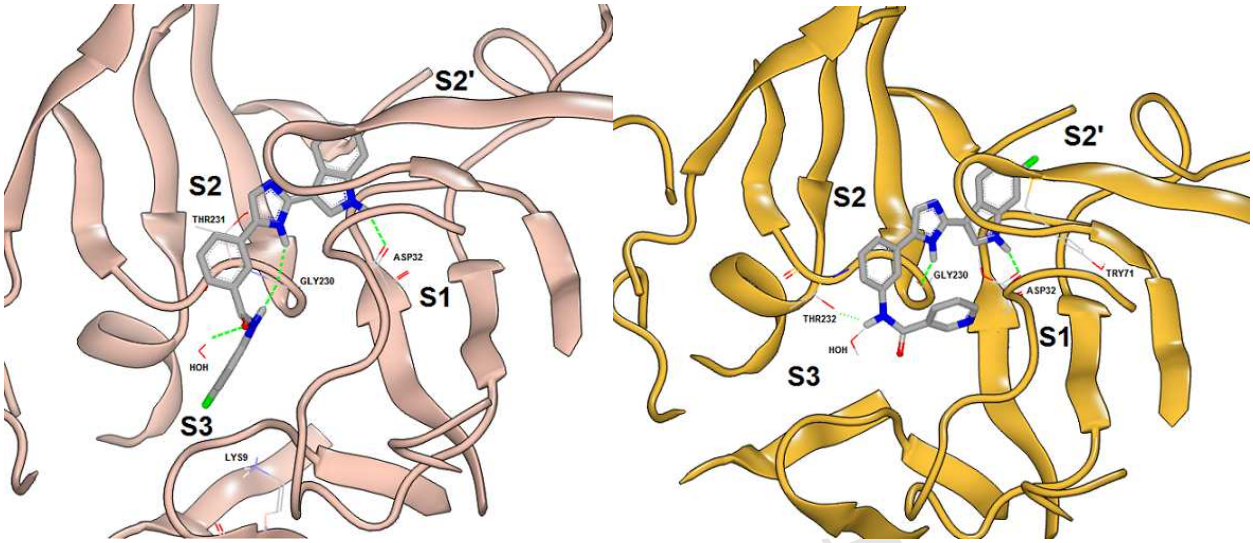

(A) **(B)**

Figure 5. Best docked poses of compounds **5b** (**A**) and **9b** (**B**) within the active site of BACE-1 enzyme based on ensemble docking. Ligands are in stick rendering and enzyme subsites are marked for clarity. Hydrogen bond interactions are shown as green dashed lines.

Table 1. IC_{50} and EC_{50} values of BACE1 inhibitors.[a]

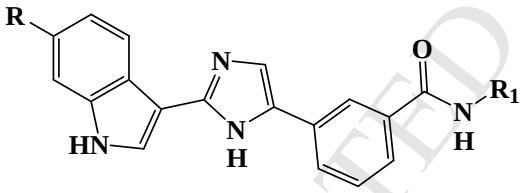

5a: R = H, R1 = Phenyl
5b: R = H, R1 = 4-flouroPhenyl
5c: R = H, R1 = 4-pyridyl
5d: R = H, R1 = 3-pyridyl

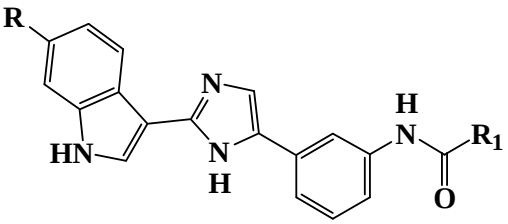

9a: R = H, R1 = 3-pyridyl
9b: R = F, R1 = 3-pyridyl

Compound	BACE1 IC_{50} (nM)	ELISA, WT EC_{50} (µM, %inh)	Binding Score	PSA (Å^2)	*Clog*P	*Log*BB
5a	110±12	1.21 (64%)	-41.26	73.6	4.62	-0.197
5b	98 ±13	1.33 (69%)	-41.29	73.6	4.78	-0.171
5c	660±21	0.59 (70%)	-39.93	86.5	3.54	-0.561
5d	310±18	0.88 (42%)	-38.68	86.5	3.54	-0.561
9a	220±15	0.48 (75%)	-41.01	86.5	3.54	-0.561
9b	130±16	0.41 (82%)	-41.84	86.5	3.70	-0.535

[a]IC_{50} and EC_{50} values are the mean values of at least three experiments ± SD.

the S1 pocket and secondly, the amidic nitrogen is engaged in different interaction with the Thr232 amino acid residue (Figure 5b). With these results in hand, we turned our attention toward finding groups that fit more properly with S1-S3 sub-pockets. Based on our earlier extensive experience in these systems, we envisioned that a more rigid imidazole ring would allow direct projection towards the unoccupied S2 sub-pocket. Therefore, we have introduced a phenyl group at 4-position of the imidazole moiety leading to compounds **10a-b** (Scheme 3), and tested those for their activity profile against BACE1 (Table 2). As expected, compounds **10a-b** were found to be more potent against BACE1 when compared to the **5** and **9** series. The activity was decreased when the fluorine atom was replaced by the OCF_3 group, however, cellular potency increased (Table 2). Upon docking using FITTED program under induced-fit mode, it was found that in the aryl-anchored imidazole derivatives **10a-b**, the isophthalic core favors its orientation towards the S2 pocket and appeared to be buried deeper into the S2 pocket (Figure 6a) with profound S2 shape complementarity. This may explain the improved potency of these rigid systems.

With these promising results in hand, we shifted our efforts towards further rigidification, as we felt that this strategy was more likely to lead to the identification of drug-like BACE1 inhibitors with the potential for good oral bioavailability and CNS penetration. Accordingly, benzimidazole-anchored derivatives **11a-b** were synthesized according to Scheme 4 and subsequently tested for their activities against BACE1 (Table 2). Fortunately, this brought about a similar potency toward BACE1; however, cellular potency was increased four-folds. As shown in Figure 6b, these derivatives showed shallower penetration into the S2 pocket with ability to form hydrogen bonding with the Lys321 residue and water molecules. In both groups, the fluorine atoms appeared to influence their appropriate projection toward the S2 pocket compared to OCF_3 group.

This analysis could explain the enhanced potency of compounds **10a-b** and **11a-b** compared to the more flexible amide series, which could be due to differences in the dynamic motion of the “Flap” loop of BACE1 upon ligand engagement. This apparently may have influenced the ligand/protein contacts and impeded the ligand’s affinity for BACE1 site, thus resulting in increased activity.

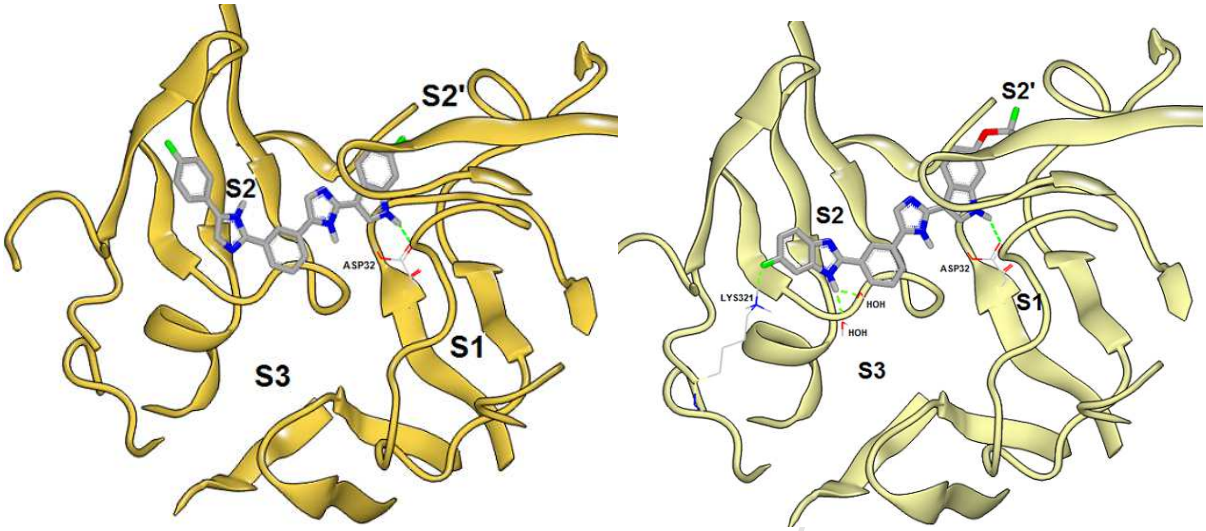

(A) **(B)**

Figure 6. Best docked poses of compounds **10a** (**A**) and **11b** (**B**) within the active site of BACE-1 enzyme based on ensemble docking. Ligands are in stick rendering and enzyme subsites are marked for clarity. Hydrogen bond interactions are shown as green dashed lines.

Table 2. IC_{50} and EC_{50} values of BACE1 inhibitors.[a]

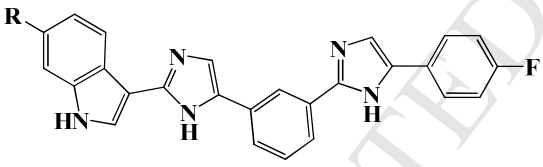

10a: R = F
10b: R = OCF_3

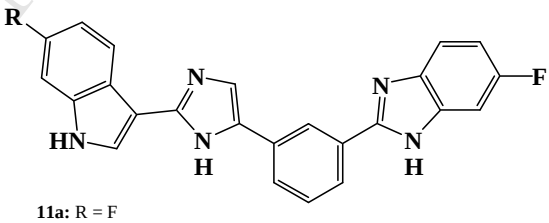

11a: R = F
11b: R = OCF_3

Compound	BACE1 IC_{50} (nM)	ELISA, WT EC_{50} (uM, %inh)	Binding Score	PSA (Å^2)	*Clog*P	*Log*BB
10a	75±9	0.81 (86%)	-39.60	73.2	5.46	-0.054
10b	180±8	0.67 (77%)	-42.42	82.4	6.67	0.005
11a	85±10	0.35(90%)	-37.29	73.2	5.22	-0.093
11b	120±9	0.29 (87%)	-43.34	82.4	6.42	-0.035

[a]IC_{50} and EC_{50} values are the mean values of at least three experiments ± SD.

With these promising results in hand, we next turned our focus toward assessing the ability of our derivatives in crossing the blood-brain barrier. It has been noted that molecules possessing a large PSA may encounter difficulty in transiting biological membranes. This inability to cross membranes may result

in poor absorption or lack of blood-brain barrier (BBB) penetration. Some of the first works correlating PSA and oral absorption were published by Kelder and Palm [24] who found that highly absorbed (>90%) drugs had a polar surface area around 70 $Å^2$ while drugs that were poorly absorbed (<10%) had a polar surface area larger than 140 $Å^2$. Furthermore, the contribution of molecular LogP to the overall BB-permeation capacity was found to be well correlated, and numerous models were reported describing such influence including that proposed by Clark [25]. For this purpose, we regenerated the previously reported Clark's equation (See supporting information) to serve as the basis for evaluating our compounds. As a result, the predicted LogBB values (Tables 1 and 2) ranged from modest -0.5 to very encouraging 0.005 value. The derivatives, **10a-b** and **11a-b**, with less polar character as indicated by their calculated LogP values, showed superior predicted penetration profile compared with the other derivatives. This indicates a plausible PSA/LogP balance characteristics favoring blood-brain penetration compared to the basic amide analogs.

These promising biological results of the aforementioned four chemically diverse collections encouraged us to find the hidden relationship that encodes the chemical features of our derivatives with respect to the observed BACE1 IC_{50}. Towards this objective, we decided to conduct a classical QSAR study by considering the logarithmic IC_{50} values of our compounds as dependent variable, and calculating *ca.* 1875 different descriptors to serve as independent variables. We found that the best developed model capable of describing the inhibitory pattern against BACE1 is illustrated by the following equation.

$$\mathbf{pIC50} = 14.0703\text{-}1.4585\times\mathbf{ATSC6c}+24.5008\times\mathbf{BCUTc_{1L}}$$

$$\mathbf{n} = 10,\ \boldsymbol{F}\text{-Statistic} = 61.15,\ \boldsymbol{R}^2 = 0.946,\ \boldsymbol{Q}^2\text{LOO} = 0.882,\ \boldsymbol{Q}^2_{\text{LMO}} = 0.869,\ \boldsymbol{R}^2_{\text{Y-scr}} = 0.215,\ \mathbf{s} = 0.076$$

Where, the first descriptor, ***ATSC6c***, is the centered Broto-Moreau autocorrelation of lag 6 weighted by atomic charges. It is basically the spatial autocorrelation over the 2D molecular graph and describes how atomic charges are distributed along the topological structure. On the other hand, the ***BCUTc-1l*** descriptor is the number of highest eigen-values with respect to lowest partial charge weighted BCUTS. This descriptor is based on the earlier modified burden matrix taking into account molecular connectivity as well as the Gasteiger-Marsilli atomic partial charges.

The illustrated model was found to fit the experimental IC_{50} values (Figure 7) with considerable level of significance as indicated by its high Fischer's value (F), squared correlation coefficients (R^2) and the

minor standard errors of estimate. The model internal predictive power was judged based on leave-one-out (LOO) and leave-many-out (LMO) procedures. The probability of chance correlation was examined by Y-scrambling, in which lower ($R^2_{Y\text{-}Scr}$) value indicates lesser probability of chance correlation. The internal validation parameters fulfilled the predicted model and demonstrated the reliability and robustness in predicting new derivatives within our series and can be utilized for future development.

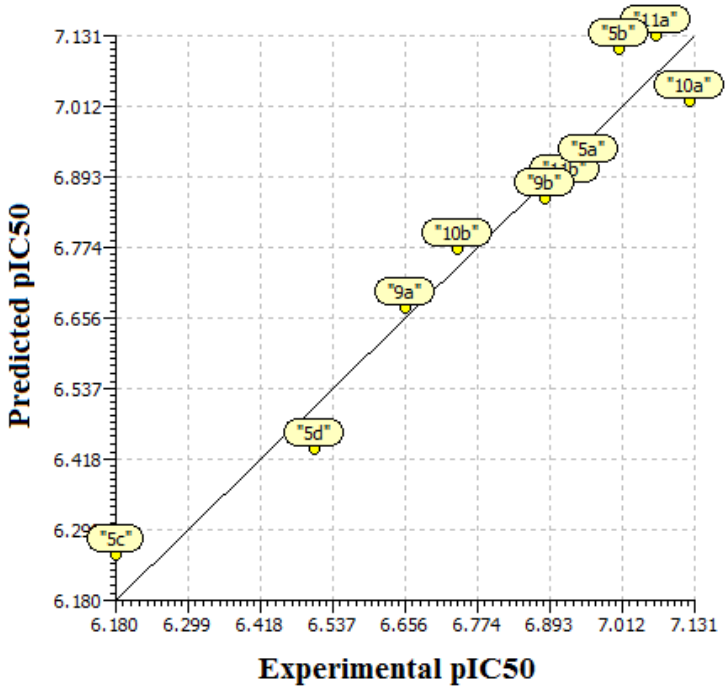

Figure 7. Scatter plot of Experimental *versus* predicted bioactivities (expressed by pIC_{50}) against BACE1 enzyme derived from the best QSAR.

3. CONCLUSION

In this work we have optimized the synthesis of novel, low molecular weight and potent transition state inhibitors of BACE1. Furthermore, we have developed peptido-mimetic groups to replace P1-P1' and P3 moieties resident on compound **I**. The synthetic methodologies followed were simple, efficient and economic. Several of the developed low molecular weight scaffolds possessed high affinity, promising ligand efficiency and acceptable PSA/LogP balance. Many of these motifs exhibited comparable cellular potency. Moreover, since the peptidic nature and the number of rotatable bonds of these motifs are low, the designed scaffolds represent a novel class of drug-like leads. The results described here merit further investigations and developments in our laboratories.

4. EXPERIMENTAL SECTION

4.1. General Methods

All reagents were used as purchased from commercial suppliers without further purification. The reactions were carried out in oven-dried or flamed graduated vessels. Solvents were dried and purified by conventional methods prior use. Flash column chromatography was performed with silica gel 60, 0.040-0.063 mm (230-400 mesh). Aluminum-backed plates pre-coated with silica gel 60 (UV254) were used for thin layer chromatography. ^{1}H and ^{13}C NMR spectra were recorded on a 400 MHz/100 MHz spectrometer. Splitting patterns are designated as s, singlet; d, doublet; t, triplet; q, quartet; m, multiplet; br, broad. Chemical shifts (δ) are given in ppm relative to the resonance of their respective residual solvent peak, CD_3OD. High and low resolution mass spectroscopic analyses were conducted using positive ion mode by Electrospray Ionization (ESI). The samples were dissolved in acetonitrile, diluted in spray solution (methanol/water 1:1 v/v + 0.1% formic acid) and infused using a syringe pump with a flow rate of 2 μL/min. External calibration was conducted using the arginine cluster in a mass range m/z 175-871.

4.2. Chemistry

*4.2.1. General procedures for the synthesis of compounds **5a-d** and **11a-b***: To a solution of 3-(2-(1H-indol-3-yl)-1H-imidazol-5-yl) benzoic acid (**4**) (303 mg, 1 equiv) in DMF (8 mL) at 0 ^{o}C was added DIPEA (0.21 mL, 1.2 mmol, 1.2 equiv). After 10 min, TBTU (551 mg, 1.2 mmol, 1.2 equiv) was added and the resulting mixture stirred at the same temperature for 30 min. Then the desired aniline or diaminobenzene (1.1 mmol, 1.1 equiv) was added. The resulting mixture was stirred at 0 ^{o}C for 4 h, and then quenched with ice-water. The precipitated solid was filtered, washed with water and dissolved in EtOAc. The organic phase was washed with a 1 N HCl aqueous solution, then with a saturated $NaHCO_3$ aqueous solution, and finally H_2O, dried over $MgSO_4$, and concentrated in vacuo, which was used in the next stage without further purification. For **5a-b**, the crude product was purified by silica gel flash chromatography using increasing concentrations of DCM/AcOEt. For the synthesis of compounds **11a-b**, to the amides from the previous step, was added AcOH (30 mL) and the resulting suspension was refluxed for 5 h, cooled to room temperature, concentrated in vacuo and diluted with crushed ice. The brown solid was filtered, washed thoroughly with water. The crude was dissolved in EtOAc washed with a saturated $NaHCO_3$ aqueous solution and with H_2O, dried over $MgSO_4$, and concentrated in vacuo. The

crude product was purified by flash chromatography on silica gel (DCM/AcOEt, 8/2 to 7/3) to give benzimidazole derivatives **11a**-**b**.

*4.2.2. General procedures for the synthesis of compounds **4a**-**4b** and **10a**-**10b**:* To a solution of 1H-indole-3-carboxylic acid (**3**) (161 mg, 1.0 mmol, 1 equiv) in DMF (10 mL) or 3-(2-(1H-indol-3-yl)-1H-imidazol-5-yl)benzoic acid (**4**) (303 mg, 1 equiv) at 0 ^{o}C was added DIPEA (0.21 mL, 1.2 mmol, 1.2 equiv). The resulting mixture was stirred at 0 ^{o}C for 30 min followed by dropwise addition of the appropriate α-bromoketone (1.1 mmol, 1.1 equiv) in DMF. The resulting mixture was stirred at 0 ^{o}C for 4 h, and then quenched with ice-water. The precipitated solid was filtered, washed with water and dissolved in EtOAc. The organic phase was washed with a 1 N HCl aqueous solution, and then a saturated $NaHCO_3$ aqueous solution, then H_2O, dried over $MgSO_4$, and concentrated in vacuo, which was used in the next stage without further purification. To this product, AcOH (25 mL) and $AcONH_4$ (924 mg, 12 mmol, 12 equiv) was added and the resulting suspension was refluxed for 5 h, cooled to room temperature, concentrated in vacuo and diluted with crushed ice. The brown solid was filtered, washed thoroughly with water. The crude cake was dissolved in EtOAc washed with a saturated $NaHCO_3$ aqueous solution and with H_2O, dried over $MgSO_4$, and concentrated in vacuo. The crude product was purified by flash chromatography on silica gel (DCM/EtOAc, 8/2 to 7/3) to give imidazole derivatives **4a**-**4b** or **10a**-**10b**.

*4.2.3. General procedures for the synthesis of compounds **9a**-**b***: To a solution of of 1H-indole-3-carboxylic acid (**3**) (161 mg, 1.0 mmol, 1 equiv) in DMF (10 mL) or 3-(2-(1H-indol-3-yl)-1H-imidazol-5-yl)benzoic acid (**4**) (303 mg, 1 equiv) at 0 ^{o}C was added DIPEA (0.21 mL, 1.2 mmol, 1.2 equiv). The resulting mixture was stirred at 0 ^{o}C for 30 min followed by dropwise addition of the appropriate α-bromoketone (1.1 mmol, 1.1 equiv) in DMF. The resulting mixture was stirred at 0 ^{o}C for 4 h, and then quenched with ice-water. The precipitated solid was filtered, washed with water and dissolved in EtOAc. The organic phase was washed with a 1 N HCl aqueous solution, and then a saturated $NaHCO_3$ aqueous solution, then H_2O, dried over $MgSO_4$, and concentrated *in-vacuo*, which was used in the next stage without further purification. To this product, AcOH (25 mL) and $AcONH_4$ (924 mg, 12 mmol, 12 equiv) was added and the resulting suspension was refluxed for 5 h, cooled to room temperature, concentrated in vacuo and diluted with crushed ice. The brown solid was filtered, washed thoroughly with water. The crude cake was dissolved in EtOAc washed with a saturated $NaHCO_3$ aqueous solution and with H_2O, dried over $MgSO_4$, and concentrated in vacuo. The crude product was purified by flash chromatography on silica gel (DCM/EtOAc, 8/2 to 7/3) to give nitro imidazole derivatives **8a**-**b**. To this product (1 mmol)

in MeOH (10 ml) was added HCO_2NH_4 (4 mmol) and Pd/C (10%wt/wt) and DMF (0.1 ml) and the mixture was heated to 70 ^oC for 1h, filtered over celite, evaporated to dryness. The crude solid was dissolved in EtOAc and washed with a saturated $NaHCO_3$ aqueous solution, then H_2O, dried over $MgSO_4$, and concentrated in vacuo, which was used in the next stage without further purification. The amine product (1 mmol) was dissolved in DMF (8 mL) at 0 ^oC followed by the adition of DIPEA (0.21 mL, 1.2 mmol, 1.2 equiv). After 10 min, TBTU (551 mg, 1.2 mmol, 1.2 equiv) was added and the resulting mixture stirred at the same temperature for 30 min. Then the desired benzoic acid (1.1 mmol, 1.1 equiv) was added. The resulting mixture was stirred at 0 ^oC for 4 h, and then quenched with ice-water. The precipitated solid was filtered, washed with water and dissolved in EtOAc. The organic phase was washed with a 1 N HCl aqueous solution, then with a saturated $NaHCO_3$ aqueous solution, and finally H_2O, dried over $MgSO_4$, and concentrated in vacuo, which was purified by flash chromatography on silica gel (DCM/EtOAc) to give amide derivatives **9a**-**b**.

4.2.4. 3-(2-(1H-Indol-3-yl)-1H-imidazol-5-yl)-N-phenylbenzamide (**5a**)

This derivative was synthesized according to the general procedure C. Yield 55%, white solid. ^{1}HNMR (CD_3OD, 400 MHz, in ppm): δ = 8.18 (1H, m), 7.32 (5H, m) 7.19 (3H, m), 7.04 (3H, m), 6.94(2H, m), 6.63(2H, m). ^{13}C NMR (100 MHz, CD_3OD, in ppm): δ 161.2, 150.3, 137.1, 133.8, 132.7, 127.9, 125.3, 125.0, 124.7, 123.3, 122.2, 121.2, 120.7, 119.6, 117.4, 115.6, 112.5, 112.2. HRMS (ESI): calcd. for $C_{24}H_{18}N_4O$ $[M]^+$: 378.1481; found 378.1451.

4.2.5. 3-(2-(1H-Indol-3-yl)-1H-imidazol-5-yl)-N-(4-fluorophenyl)benzamide (**5b**)

This derivative was synthesized according to the general procedure C. Yield 63%, white solid. ^{1}HNMR (CD_3OD, 400 MHz, in ppm): δ = 8.18 (1H, s), 7.63 (3H, m) 7.26 (m, 3H), 7.19 (m, 4H), 7.10 (1H, t, *J* = 6.7 Hz), 7.02 (2H, m). ^{13}C NMR (100 MHz, CD_3OD, in ppm): δ 161.2, 157.9, 150.3, , 139.1, 136.3, 132.7, 129.2, 128.8,127.7, 126.9, 126.3, 125.3, 125.0, 124.1, 123.3, 122.3, 121.0, 121.2, 120.9, 119.5, 119.3, 117.4, 116.3, 115.9, 112.5, 108.2. HRMS (ESI): calcd. for $C_{24}H_{17}FN_4O$ $[M]^+$: 396.1386; found 396.1381.

4.2.6. 3-(2-(1H-Indol-3-yl)-1H-imidazol-5-yl)-N-(pyridin-4-yl)benzamide (**5c**)

This derivative was synthesized according to the general procedure C. Yield 45%, white solid. ^{1}HNMR (CD_3OD, 400 MHz, in ppm): δ = 8.64 (2H, d, *J* = 8.1 Hz) , 8.11(4H, m), 8.02(1H, s) 7.82 (5H, m), 7.64(2H, t, *J* = 7.1 Hz), 7.14(1H, t, *J* = 7.4 Hz). ^{13}C NMR (100 MHz, CD_3OD, in ppm): δ 166.6, 148.4, 148.2,

147.9, 146.5, 146.1, 137.4, 131.2, 130.7, 130.3, 128.2, 127.8, 126.2, 125.7, 123.2, 121.3, 119.8, 118.9, 115.9, 114.7, 114.4, 112.5, 112.3. HRMS (ESI): calcd. for $C_{23}H_{17}N_5O$ $[M]^+$: 379.1433; found 379.1435.

4.2.7. 3-(2-(1H-Indol-3-yl)-1H-imidazol-5-yl)-N-(pyridin-3-yl)benzamide (**5d**)

This derivative was synthesized according to the general procedure C. Yield 71%, white solid. ^{1}HNMR (CD_3OD, 400 MHz, in ppm): δ = 9.09 (1H, s),8.45 (1H, d, *J* = 7.4 Hz), 8.37 (1H, dd, *J* =1.2, 6.7 Hz), 8.07(3H, m),8.10(1H, s),7.93 (2H, m),7.84(1H,t, *J* =7.2 Hz), 7.72 (2H, m),7.57(1H, dd, *J* = 6.7, 8.3 Hz), 7.21(1H, t, J = 8.2 Hz). ^{13}C NMR (100 MHz, CD_3OD, in ppm): δ 167.1, 147.2, 144.1, 141.4, 140.1, 137.4, 134.2, 133.2, 130.9, 130.1, 129.4, 128.3, 127.6, 126.5, 125.9, 125.2, 124.4, 122.7, 120.4, 119.2, 116.3, 112.7, 112.5. HRMS (ESI): calcd. for $C_{23}H_{17}N_5O$ $[M]^+$: 379.1433; found 379.1421.

4.2.8. N-(3-(2-(1H-Indol-3-yl)-1H-imidazol-5-yl)phenyl)isonicotinamide (**9a**)

This derivative was synthesized according to the general procedure C. Yield 69%, white solid. ^{1}HNMR (CD_3OD, 400 MHz, in ppm): δ = 8.92 (1H, s) 8.70 (1H, t, *J* = 3.8 Hz), 8.61(1H, d, *J* = 7.1 Hz), 8.34 (1H, s), 8.13 (3H, m), 8.07 (1H, s), 7.79 (1H, d, *J* = 7.2 Hz), 7.67 (2H, m), 7.53 (1H, t, *J* = 3.5 Hz), 7.41(1H, dd, *J* = 3.8, 7.4 Hz) , 7.19 (1H, t, *J* = 7.3 Hz). ^{13}C NMR (100 MHz, CD_3OD, in ppm): δ 163.7, 154.1, 147.4, 147.1, 143.5, 138.7, 137.5, 137.2, 133.4, 132.2, 131.1, 127.5, 125.1, 123.2, 121.4, 120.3, 119.2, 118.9, 118.2, 115.7, 113.1, 112.7. HRMS (ESI): calcd. for $C_{23}H_{17}N_5O$ $[M]^+$: 379.1433; found 379.1430.

4.2.9. N-(3-(2-(6-Fluoro-1H-indol-3-yl)-1H-imidazol-5-yl)phenyl)nicotinamide (**9b**)

This derivative was synthesized according to the general procedure C. Yield 58%. ^{1}HNMR (CD_3OD, 400 MHz, in ppm): δ = 9.00 (1H, s), 8.71(1H, t, *J* = 3.7 Hz), 861(1H, d, *J* = 7.1 Hz), 8.39 (1H , s), 8.13 (2H, m), 8.10 (1H, s),7.99 (1H, d, *J* = 7.2 Hz), 7.84(1H, d, *J* = 7.3 Hz), 7.54 (2H, m) 7.43(1H, dd, *J* = 6.9, 7.3 Hz), 7.14 (1H, dd, *J* = 3.2,6.7 Hz). ^{13}C NMR (100 MHz, CD_3OD, in ppm): δ 164.1, 157.9, 154.3, 153.8, 149.7, 148.4, 147.9, 139.5, 139.2, 138.8, 137.7, 134.5, 133.2, 131.3, 124.7, 123.4, 122.9, 119.1, 118.4, 114.1, 113.2, 109.1, 104.5. HRMS (ESI): calcd. for $C_{23}H_{16}FN_5O$ $[M]^+$: 397.1339; found 397.1341.

4.2.10. 6-Fluoro-3-(5-(3-(5-(4-fluorophenyl)-1H-imidazol-2-yl)phenyl)-1H-imidazol-2-yl)-1H-indole (**10a**)

This derivative was synthesized according to the general procedure C. Yield 67%. ^{1}HNMR (CD_3OD, 400 MHz, in ppm): δ = 8.52(1H, d, *J* = 8.1 Hz), 8.16 (1H, t, *J* = 7.9 Hz), 8.07 (2H, d, *J* = 3.4 Hz), 7.41 (1H, s),

7.39 (2H, m),7.18 (1H, d, *J* = 7.4 Hz), 7.16 (1H, d, J = 7.1 Hz), 6.93 (1H, dd, *J* = 4.74 Hz), 6.90 (3H, m), 6.67 (1H, dd, *J* = 1.3, 3.2, 6.5 Hz). ^{13}C NMR (100 MHz, CD_3OD, in ppm): δ 160.2, 159.4, 155.9, 150.3, 150.0, 140.2, 136.9, 132.5, 132.4, 129.8, 129.7, 128.7, 126.2, 125.5, 124.0, 123.8, 123.7, 118.2, 117.4, 114.3, 111.7, 108.2, 102.5, 102.7. HRMS (ESI): calcd. for $C_{26}H_{17}F_2N_5$ $[M]^+$: 437.1452; found 437.14492.

4.2.11. 3-(5-(3-(5-(4-Fluorophenyl)-1H-imidazol-2-yl)phenyl)-1H-imidazol-2-yl)-6-(trifluoromethoxy)-1H-indole (**10b**)

This derivative was synthesized according to the general procedure C. Yield 60%, white solid. ^{1}HNMR (CD_3OD, 400 MHz, in ppm): δ = 8.47 (1H, d, *J* = 8.1 Hz), 8.31(1H, t, *J* = 7.3 Hz), 8.03 (2H, m), 8.11(1H, s), 8.06 (1H, s), 7.73 (1H, d, *J* = 7.4 Hz), 7.70 (2H, m), 7.16 (1H, m), 6.90 (1H, bs), 6.80 (1H, bs). ^{13}C NMR (100 MHz, CD_3OD, in ppm): δ 159.4, 156.8, 155.9, 153.2, 150.3, 147.4, 146.7, 145.9, 139.9, 136.7, 134.7, 129.7, 128.2, 127.0, 126.0, 125.7, 125.0, 123.8, 121.5, 117.4, 116.2, 116.1, 112.0, 111.8, 108.2, 102.5, 102.2. HRMS (ESI): calcd. for $C_{27}H_{17}F_4N_5O$ $[M]^+$: 503.1369; found 503.1372.

4.2.12. 6-Fluoro-2-(3-(2-(6-fluoro-1H-indol-3-yl)-1H-imidazol-5-yl)phenyl)-1H-benzo[d]imidazole (**11a**)

This derivative was synthesized according to the general procedure C. Yield 51%, white solid. ^{1}HNMR (CD_3OD, 400 MHz, in ppm): δ = 8.36 (1H, s), 8.01(1H, d, *J* = 7.1 Hz) , 7.91 (1H, d, *J* = 7.7 Hz), 7.69 (3H, m), 7.61 (2H, bs), 7.51 (4H, m), 7.12 (3H, m). ^{13}C NMR (100 MHz, CD_3OD, in ppm): δ 159.4, 156.8, 159.9, 153.3, 150.3, 139.9, 135.7, 134.7, 128.2, 127.0, 126.4, 125.6, 125.0, 123.8, 121.5, 121.5, 117.4, 116.2, 112.0, 111.8, 108.2, 102.5, 102.2. HRMS (ESI): calcd. for $C_{24}H_{15}F_2N_5$ $[M]^+$: 411.1295; found 411.1299.

4.2.13. 6-Fluoro-2-(3-(2-(6-(trifluoromethoxy)-1H-indol-3-yl)-1H-imidazol-5-yl)phenyl)-1H-benzo[d]imidazole (**11b**)

This derivative was synthesized according to the general procedure C. Yield 73%, white solid. ^{1}HNMR (CD_3OD, 400 MHz, , in ppm): δ = 9.121 (1H, bs), 8.74(1H, s), 8.34 (1H, d, *J* = 7.4 Hz), 8.12 (2H, m), 8.27 (1H, s), 8.02 (1H, d, *J* = 3.8 Hz), 7.91 (1H, dd, *J* = 1.4, 7.4 Hz), 7.70 (2H, m), 7.50 (2H, m), 7.34 (1H, dd, *J* = 3.4, 7.3 Hz), 7.12 (2H, m). ^{13}C NMR (100 MHz, CD_3OD, in ppm): δ 160.0, 156.6, 153.2, 150.3, 149.0, 142.8, 138.1, 135.7, 127.0, 126.4, 125.7, 125.0, 123.0, 122.9, 122.4, 121.5, 117.4, 112.9, 112.5, 109.8, 109.7, 103.9, 103.5, 98.8. HRMS (ESI): calcd. for $C_{25}H_{15}F_4N_5O$ $[M]^+$: 477.1213; found 477.1220.

4.3. Biology

4.3.1. BACE1 Enzymatic Assay

BACE1 assay was carried out according to the manufacturer described protocol available from Invitrogen, USA (http://tools.invitrogen.com/content/sfs/manuals/L0724.pdf). Briefly, BACE1 *in-vitro* assay was carried out by fluorescence resonance energy transfer (FRET). An APP-based peptide substrate (rhodamine-EVNLDAEFK-quencher, K_M value of 20 µM) carrying the Swedish mutation and containing a rhodamine as a fluorescence donor and a quencher acceptor at each end was used. The intact substrate is weakly fluorescent and becomes highly fluorescent upon enzymatic cleavage. The assays were conducted for both enzymes in 50 mM sodium acetate buffer pH 4.5, in a final enzyme concentration (1 U/mL), inhibitor (first line screening: 30 µM, 10 µM, 3 µM, 1 µM, and 0.3 µM) compounds that showed high activity at 0.3 µM were validated at low concentration and both substrates were used at a concentration of 750 nM. Inhibitor compounds were diluted from stock solutions to result in 3.3% DMSO final concentration. The reaction was incubated for 60 min at 25 °C under dark conditions and then stopped with 2.5 M sodium acetate. Fluorescence measured with a Victor^3 1420 (Wallac) microplate reader at 545 nm excitation and 585 nm emissions. The assay kit was validated by manufacturer. The obtained values are the mean values of 3 different experiments. IC_{50} values were calculated by plotting the obtained relative fluorescence unit per hour (RFU/h) against the logarithmic of inhibitor concentration. The measured inhibition data were analyzed in GraphPad Prism 4 for Windows (GraphPad Software Inc., La Jolla, USA) by nonlinear regression (curve fitting).

4.3.2. Cell based assay

Aβ42 and Aβ40 were measured in culture medium of H4 cells (human neuroglioma cell line), expressing the double Swedish mutation (K595N/M596L), of human APP (APPsw). Cells were seeded onto 24-well plates (2x105 cell well-1) and allowed to grow for 24h, in 5% CO_2/95% air in humidified atmosphere. Increasing concentrations of compounds were added to the cells for overnight in a final volume of 0.5 ml. *R*-flurbiprofen was used as positive control. DMSO-d6 (1%) was used as negative control. At the end of the incubation, 100 µl of supernatants were removed and treated with a biotinylated mouse monoclonal antibody (4G8, Signet Laboratories Inc., Dedham, MA, USA), specifically recognizing the 17-24 amino acid region of Aβ and two rabbit polyclonal antibodies (C-term 42 and C-term 40, BioSource International, Camarillo, CA, USA), specifically recognizing the C-terminus of Aβ42and Aβ40, respectively. Antigen–antibodies 5 complexes were recognized by TAG-donkey anti-rabbit IgG (Jackson

Immuno Research Laboratories, Soham, UK). Streptavidin coated magnetic beads captured the complexes and the signals were read by an electrochemiluminescence instrument (Origen M8 Analyzer, BioVeris Corporation, Gaithersburg, MD, USA). The cytotoxicity potential of test compound was assessed in the same cells of the Aβ assay using the 3-[4,5-dimethylthiazol-2-yl]-2,5-diphenyltetrazol-iumbromide (MTT) assay. After medium removal for of Aβ42 and Aβ40 determination, cells were incubated for 3h with 500µl culture medium containing 0.5 mg ml-1 MTT, at 37 ºC, 5% CO_2 and saturated humidity. After removal of the medium, 25-500µl of 100% DMSO-d6 were added to each well. The amount of formed formazan was determined reading the samples at 570 nm (background 630 nm) using a microplater reader (model 450, Bio-Rad, Hercules, CA, USA).

4.4. Molecular Modeling

4.4.1. Molecular Docking

The binding modes for the synthesized compounds were explored by means of fully flexible molecular docking computations employing the FITTED Suite, version 3.6 [23]. A well resolved X-ray crystal structures for human beta secretase complexed with potent inhibitors were retrieved from the protein data bank (http://www.rcsb.org/pdb/) under the entry codes (1TQF, 2B8L, 2QZL and 3EXO). Our compounds were drawn using ChemBioDraw Ultra, version 11 (http://www.cambridgesoft.com) and were optimised for energy and geometry using MMFF94s force field. Next, the compounds were prepared for docking by assigning the proper bond orders, atom types, hybridization, partial atomic charges using the SMART module within FITTED Suite.

The β-secretase crystal structures were subjected to a number of automated preparation steps prior docking employing the different FITTED Suite modules. The PREPARE module was utilized to perform sequence alignment, deletion and mutation to ensure that all of the protein ensembles are similar and differ only by their Cartesian coordinates. Subsequently, MOL2 files for the different proteins ensembles including water molecules apart from their complexed inhibitors were optimised for energy and orientation by adding hydrogens, identifying alternative conformations and protonation states. The catalytic Asp 32 residue was kept protonated during this procedure [26]. Later, the different protein conformations were processed using ProCESS module to generate a truncated cavity and interaction site within 10 Å from the center of the binding site and to identify the flexible residues within such dimensions. Each of our compounds was docked individually using FITTED program under a fully

flexible mode using the default parameters. The program accounts for the flexibility of protein/ligand complexes *via* an hybrid matching/genetic algorithm search engine (i.e., evolution, mutation and crossover) allowing water molecules to be exchanged independently from the different protein backbones. Such computations provided an Induced-Fit like approach that simulates reality in biological environment. The optimal binding mode for each compound was identified according to the lowest energy complex emerged after each run. Finally, the results were presented using OpenEye VIDA [27] specialized 3D molecular docking results viewer.

4.4.2. Quantitative-Structure Activity Relationship

The studied compounds were drawn using ChemBioDraw Ultra 11 (http://www.cambridgesoft.com) and for each compound, the lowest energy conformation was obtained by means of MOPAC2012 program [28] embedded within VEGA-ZZ [29-30]. The accurate energy minimization was achieved by Austin Model-1 (AM1) semiemperical force-field within MOPAC. The AM1 force-field is characterized by its high accuracy and coverage for wide range of atoms. Molecular descriptors calculations were carried-out using PaDEL-Descriptor software [31]. The software calculates a large set of 1D-3D molecular descriptors (*ca.* 1875) of different classes including constitutional, topological, information indices, eigenvalue-based indices, radial distribution function (RDF), 2D/3D autocorrelation..*etc*. The calculated descriptors were served as independent variables during QSAR model development. The logarithmic values of experimentally observed IC_{50} values were served as the dependent variable. The QSAR models were developed and validated employing the QSARINS software [32-33]. Model development process initiated by reducing co-linear variables (corr. > 0.98) and excluding the descriptor showing higher pair-wise correlation with others. All subsets procedure was adapted for the variables selection. Multiple linear regression (GA-MLR) method was used for the final model building. The final models robustness were validated employing internal predictive measures based on Q^2_{LOO} (leave one-out), Q^2_{LMO} (leave many-out) and $R^2_{Y\text{-}scr}$ (Y-scrambling).

4.4.3. Evaluation of Blood-Brain Permeation

The ability of the synthesized compounds for targeting the central nervous system and permeating the blood-brain barrier was assessed computationally employing the previously reported Clark's equation [25]. For the original compound's training set found in Clark's paper, both the polar surface area (PSA) and

ClogP were recalculated using Marvin, version 5.8.2 (http://www.chemaxon.com). Subsequently, the QSAR equation was regenerated using QSARins software, where such regeneration was carried out to account for the difference between the PSA and ClogP used by Clark and those generated by Mervin as such difference would affect the corresponding descriptor's coefficients. The resulted QSAR equation (see supporting information) was applied to predict the (*Log*BB) of our compounds.

5. Acknowledgement

The authors would like to thank Molecular Forecaster/McGill University as well as to Prof. Paola Gramatica for providing the licensed software. This work was supported by generous grants from AlJalila Foundation, UAE (grant number AJF201531); the Vice Chancellor's office of Research and Graduate Studies-University of Sharjah-UAE (grant number 15011101007), and the KEF Holding Charity Foundation (Faizal and Shabanah Foundation)-UAE.

6. References

[1] M. Citron, Strategies for disease modification in Alzheimer's disease**,** Nat. Rev. Neurosci. 5 (9) (2004) 677-685.

[2] A. Wimo, L. Jönsson, J. Bond, M. Prince, B. Winblad B, The worldwide economic impact of dementia 2010, Alzheimers Dement. 9 (1) (2013) 1–11.

[3] Alzheimer's Association, 2009 Alzheimer's disease facts and figures, Alzheimers Dement. 5 (3) (2009) 234–270.

[4] D. J. Selkoe, Toward a comprehensive theory for Alzheimer's disease. Hypothesis: Alzheimer's disease is caused by the cerebral accumulation and cytotoxicity of amyloid beta-protein, Ann. N.Y. Acad. Sci. 924 (2000) 17-25.

[5] C. M. Couglan, K. C. Breen, Factors influencing the processing and function of the amyloid beta precursor protein—a potential therapeutic target in Alzheimer's disease?, Pharmacol. Ther. 86 (2) (2000) 111-144.

[6] M. Racchi, S. Govone, Rationalizing a pharmacological intervention on the amyloid precursor protein metabolism, Trends Pharmacol. Sci. 20 (1999) 418-423.

[7] F. Checler, Processing of the β-Amyloid Precursor Protein and Its Regulation in Alzheimer's Disease, J. Neurochem. 65 (4) (1995) 1431-1444.

[8] D. J. Selkoe, D. Schenk, Alzheimer's disease: molecular understanding predicts amyloid-based therapeutics, Annu. Rev. Pharmacol. Toxicol. 43 (2003) 545–584.

[9] J. Hardy, D. J. Selkoe, The amyloid hypothesis of Alzheimer's disease: progress and problems on the road to therapeutics, Science 297 (2002) 353–356.

[10] T. Arendt, Alzheimer's disease as a disorder of mechanisms underlying structural brain self-organization, Neuroscience 102 (4) (2001) 723-765.

[11] D.W. Dickson, The pathogenesis of senile plaques, J. Neuropathol. Exp. Neurol. 56 (4) (1997) 321-39.

[12] (a) J. Yuan, S. Venkatraman, Y. Zheng, B. M. McKeever, L. W. Dillard, S. B. Singh, Structure-based design of β-site APP cleaving enzyme 1 (BACE1) inhibitors for the treatment of Alzheimer's disease, J. Med. Chem. 56 (11) (2013) 4156-80; (b) S. Shangguan, F. Wang, Y. Liao, H. Yu, J. Li, W. Huang, H. Hu, L. Yu, Y. Hu, R. Sheng, Design, Synthesis and Evaluation of 3-(2-Aminoheterocycle)-4-benzyloxyphenylbenzamide Derivatives as BACE-1 Inhibitors, Molecules 18 (3) (2013) 3577-3594.

[13] S. Butini, E. Gabellieri, M. Brindisi, S. Giovani, S. Maramai, G. Kshirsagar, E. Guarino, S. Brogi, V. La Pietra, M. Giustiniano, L. Marinelli, E. Novellino, G. Campiani, A. Cappelli, S. Gemma, A stereoselective approach to peptidomimetic BACE1 inhibitors, Eur. J. Med. Chem. 70 (2013) 233-247.

[14] M. Faraz Khan, M. M. Alam, G. Verma, W. Akhtar, M. Akhter, M. Shaquiquzzaman, The therapeutic voyage of pyrazole and its analogs: A review, Eur. J. Med. Chem. 120 (2016) 170-201.

[15] D. Dominguez, J. Tournoy, D. Hartmann, T. Huth,K. Cryns, S. Deforce, L. Serneels, I. E. Camacho, E. Marjaux, K. Craessaerts, A. J. M. Roebroek, M. Schwake, R. D'Hooge, P. Bach, U. Kalinke, D. Moechars, C. Alzheimer, K. Reiss, P. Paul Saftig, B. De Strooper, Phenotypic and biochemical analyses of BACE1- and BACE2-deficient mice, J. Biol. Chem. 280 (35) (2005) 30797–30806.

[16] CoMentis. Press release 28 Jul 2008: CoMentis and Astellas to present Alzheimer's disease research at International Conference on Alzheimer's Disease (ICAD). CoMentis website [online], http://www.athenagen.com/index.php?/athenagen/press_releases/52/ (2008).

[17] D. Leung, G. Abbenante, D. P. Fairlie, Protease inhibitors: current status and future prospects, J. Med. Chem. 43 (3) (2000) 305–341.

[18] T.B. Durham, T. A. Shepherd, Progress toward the discovery and development of efficacious BACE inhibitors, Curr. Opin. Drug Discov. Develop. 9 (6) (2006) 776–791.

[19] T. H. Al-Tel, R. A. Al-Qawasmeh, M. F. Schmidt, A. Al-Aboudi, S. N. Rao, S. S. Sabri, W. Voelter, Rational design and synthesis of potent dibenzazepine motifs as β-secretase inhibitors, J. Med. Chem. 52 (20) (2009) 6484–6488.

[20] T. H. Al-Tel, M. H. Semreen, R. A. Al-Qawasmeh, M. F. Schmidt, R. El-Awadi, M. Ardah, R. Zaarour, S. N. Rao, O. El-Agnaf, Design, Synthesis, and Qualitative Structure–Activity Evaluations of Novel β-Secretase Inhibitors as Potential Alzheimer's Drug Leads, J. Med. Chem. 54 (24) (2011) 8373–8385.

[21] Y. Xu, M. Li, H. Greenblatt, W. Chen, A. Paz, O. Dym, Y. Peleg, T. Chen, X. Shen, J. He, H. Jiang, I. Silman, J. L. Sussman, Flexibility of the flap in the active site of BACE1 as revealed by crystal structures and molecular dynamics simulations, Acta Crystallogr D Biol Crystallogr. 68 (2012) 13-25.

[22] S.J. Stachel, C.A. Coburn, S. Sankaranarayanan, E. A. Price, B. L. Pietrak, Q. Huang, J. Lineberger, A. S. Espeseth, L. Jin, J. Ellis, M. K. Holloway, S. Munshi, T. Allison, D. Hazuda, A. J. Simon, S. L. Graham, J. P. Vacca, Macrocyclic inhibitors of beta-secretase: functional activity in an animal model, J. Med. Chem. 49 (21) (2006) 6147−6150.

[23] (a) C.R. Corbeil, P. Englebienne, N. Moitessier, Docking Ligands into Flexible and Solvated Macromolecules. 1. Development and Validation of FITTED 1.0, J. Chem. Inf. Model. 47 (2007) 435–449. (b) C. R. Corbeil, P. Englebienne, C. G. Yannopoulos, L. Chan, S. K. Das, D. Bilimoria, L. L'Heureux, N. Moitessier, Docking Ligands into Flexible and Solvated Macromolecules. 2. Development and Application of Fitted 1.5 to the Virtual Screening of Potential HCV Polymerase Inhibitors, J. Chem. Inf. Model. 48 (2008) 902–909. (c) http://fitted.ca

[24] (a) J. Kelder, P. D. G. Grootenhuis, D. M. Bayada, L. P. C. Delbressine, J. P. Ploemen, Polar molecular surface as a dominating determinant for oral absorption and brain penetration of drugs, Pharm. Res. 16 (10) (1999) 1514−1519. (b) K. Palm, P. Stenberg, K. Luthman, P. Artursson, Polar Molecular Surface Properties Predict the Intestinal Absorption of Drugs in Humans, Pharm. Res. 14 (5) (1997) 568−571.

[25] D. E. Clarck, Rapid calculation of polar molecular surface area and its application to the prediction of transport phenomena. 2. Prediction of blood-brain barrier penetration, J. Phar. Sci. 88 (8) (1999) 815-821.

[26] T. Polgår, G. M. Keserü, Virtual screening for β-secretase (BACE1) inhibitors reveals the importance of protonation states at Asp32 and Asp228, J. Med. Chem. 48 (11) (2005) 3749-3755.

[27] VIDA, version 4.2.1; Open Eye Scientific software, Inc.: Santa Fe, NM.

[28] MOPAC2012, J. J. P. Stewart, Stewart Computational Chemistry, version 15.321 web: http://OpenMOPAC.net

[29] A. Pedretti , L. Villa , G. Vistoli, VEGA--an open platform to develop chemo-bio-informatics applications, using plug-in architecture and script programming, J. of Comput. Aid. Mol. Des. 18 (3) (2004) 167-73.

[30] A. Pedretti , L. Villa , G. Vistoli, Atom-type description language: a universal language to recognize atom types implemented in the VEGA program, Theor. Chem. Acc. 109 (4) (2003) 229-232.

[31] C. W. Yap, PaDEL-descriptor: an open source software to calculate molecular descriptors and fingerprints, J. of Comput. Chem. 32 (7) (2011) 1466-1474.

[32] P. Gramatica, N. Chirico, N. Papa, S. Cassani, S. Kovarich, QSARINS: A new software for the development, analysis, and validation of QSAR MLR models, J. of Comput. Chem. 34 (24) (2013) 2121-2132.

[33] P. Gramatica, S. Cassani, N. Chirico, QSARINS-chem: Insubria datasets and new QSAR/QSPR models for environmental pollutants in QSARINS, J. of Comput. Chem. 35 (13) (2014) 1036-1044.

Research Highlights

- Four new series of isophthalic acid derivatives clubbed with Indolyl-Imidazole derivatives were synthesized.
- Some of the synthesized compounds exhibited potent activity against BACE1.
- A QSAR model of the synthesized motifs was developed using QSARINS software.